Frequency and intensity of palaeofloods at the interface of Atlantic and Mediterranean climate domains

B. Wilhelm[1,2], H. Vogel[2], C. Crouzet[3,4], D. Etienne[5], F.S. Anselmetti[2]

[1]{Univ. Grenoble Alpes, LTHE, F-38000 Grenoble, France}
[2]{Institute of Geological Sciences and Oeschger Centre for Climate Change Research, Univ. of Bern, CH-3012 Bern, Switzerland}
[3]{Univ. Savoie Mont Blanc, ISTerre, F-73376 Le Bourget-du-Lac, France}
[4]{CNRS, ISTerre, F-73376 Le Bourget-du-Lac, France}
[5]{UMR INRA 42 CARRTEL, Univ. Savoie Mont Blanc, F-73376 Le Bourget du Lac, France}
Correspondence to: B. Wilhelm (bruno.wilhelm@ujf-grenoble.fr)

Abstract

The long-term response of the flood activity to both Atlantic and Mediterranean climatic influences was explored by studying a lake sequence (Lake Foréant) of the Western European Alps. High-resolution sedimentological and geochemical analysis revealed 171 event layers, 168 of which result from past flood events over the last millennium. The layer thickness was used as a proxy of intensity of past floods. Because the Foréant palaeoflood record is in agreement with the documented variability of historical floods resulting from local and mesoscale, summer-to-autumn convective events, it is assumed to highlight changes in flood frequency and intensity related to such events typical of both Atlantic (local events) and Mediterranean (meso-scale events) climatic influences. Comparing the Foréant record with other Atlantic-influenced and Mediterranean-influenced regional flood records highlights a common feature in all flood patterns that is a higher flood frequency during the cold period of the Little Ice Age (LIA, AD 1300-1900). In contrast, high-intensity flood events are apparent during both, the cold LIA and the warm Medieval Climate Anomaly (MCA, AD 950-1250). However, there is a tendency towards higher frequencies of high-intensity flood events during the warm MCA. The MCA extremes could mean that under the global warming scenario, we might see an increase in intensity (not in frequency). However, the flood frequency and intensity in course of 20th century warming trend did not change significantly. Uncertainties in

future evolution of flood intensity lie in the interpretation of the lack of 20th century extremes (transition or stable?) and the different climate forcing factors between the two periods (greenhouse gases vs. solar/volcanic eruptions).

Key-words: palaeoflood record, flood frequency, flood intensity, Atlantic influence, Mediterranean influence, last millennium

1. Introduction

Heavy rainfall events trigger mountain-river floods, one of the most significant natural hazards, causing widespread loss of life, damage to infrastructure and economic deprivation (e.g. Kundzewicz et al., 2014). This is especially the case for the Alpine area in Europe, where tourism and recent demographic development with an increasing population raise the vulnerability of infrastructure to natural hazards (e.g. Beniston and Stephenson 2004). Moreover, the current global warming is expected to lead to an intensification of the hydrological cycle and a modification of flood hazard (IPCC et al., 2013). Hence, a robust assessment of the future evolution of the flood hazard over the Alps becomes a crucial issue.

A main limitation for robust flood-hazard projections is the scarce knowledge on the underlying natural climate dynamics that lead to these extreme events (IPCC, 2013). Indeed, the stochastic nature and the rare occurrence of extreme events make the identification of trends based on instrumental data alone difficult (e.g. Lionello et al., 2012). One way of overcoming this issue is to extend flood series beyond observational data and compare these datasets with independent climatic and environmental forcing. In this purpose, many types of sedimentary archives have been studied (e.g. Luterbacher et al., 2012 and references therein). Among them lake sediments are being increasingly studied because they allow to reconstruct flood records long enough to identify the natural variability at different time scales (e.g. Noren et al., 2002; Oslegger et al., 2009; Wilhelm et al., 2012a; Czymzik et al., 2013; Glur et al., 2013; Corella et al., 2014).

In the western Alps, many lake-sediment sequences have been studied to better assess the response of the flood activity to climate variability. These studies revealed higher flood frequency of mountain streams in many regions during multi-centennial cold phases such as the Little Ice Age (Giguet-Covex et al., 2012; Wilhelm et al., 2012a; 2013; Glur et al., 2013; Wirth et al., 2013b; Amann et al., 2015). However, regarding flood intensity/magnitude,

opposite patterns appear with the occurrence of the most extreme events during warmer periods in the north (Giguet-Covex et al., 2012; Wilhelm et al., 2012b; 2013), while they occurred during colder periods in the south (Wilhelm et al., 2012a; 2015). These north-south opposite flood patterns were explained by flood-triggering meteorological processes specific to distinct climatic influences: Atlantic in the north versus Mediterranean in the south. In the north-western part of the Alps, floods at high altitude are mainly triggered by local convective events (i.e. thunderstorms) and seem to mainly depend on the temperature that would strengthen vertical processes (e.g. Wilhelm et al., 2012b; 2013). In contrast, floods in the south are mostly triggered by mesoscale events and may strongly depend on pathways and intensity of storm-tracks (e.g. Trigo and Davis, 2000; Boroneant et al., 2006; Boudevillain et al., 2009). By analogy with these results over past warm periods, the mountain-flood hazard might be expected to increase in the north-western Alps, mainly because of an enhanced flood magnitude associated to stronger convective processes. Hence, better assessing the spatial extent of the Atlantic-influenced flood pattern at high-altitude appears a crucial issue to appropriately establish hazard mitigation plans and prevent high socio-economic damages.

In this context, the present study was designed to reconstruct the flood pattern at an intermediate situation between the north-western and south-western Alps, i.e. at the climate boundary between Atlantic and Mediterranean influences. This is undertaken by reconstructing a millennium-long flood chronicle from the sediment sequence of the high-altitude Lake Foréant located in the Queyras Massif (France).

2. Regional setting

2.1. Hydro-climatic setting and historical flood record

The Queyras massif is located in between the northern and southern French Alps where the climate is influenced by the Atlantic Ocean and the Mediterranean Sea (Fig. 1). As a result, the Queyras mountain range corresponds to a transition zone of Alpine precipitation patterns in the meteorological reanalyses (Durant et al., 2009; Plaut et al., 2009) and in the simulations (Frei et al., 2006; Rajczak et al., 2013). In the Queyras, heavy precipitation events are related to either local convective phenomena (i.e. summer thunderstorms) or mesoscale convective systems. The mesoscale systems called “Lombarde-Type” or “East Return” events occur mainly from late spring to fall and result from Mediterranean humid air masses flowing

northward into the Po Plain and then westward to the Queyras Massif (e.g. Gottardi et al., 2010; Parajka et al., 2010). The humid air masses are then vigorously uplifted with the steep topography of the Queyras massif, causing an abrupt cooling of the air masses and intense precipitations. Such mesoscale precipitation events, typical of the Mediterranean climate (e.g. Buzzi and Foschini, 2000; Lionello et al., 2012), affect extensive areas and may lead to catastrophic floods at a regional scale as shown in June 1957 or October 2000 over the Queyras massif (Arnaud-Fassetta and Fort, 2004). Other numerous past flood events were documented from studies of local historical records. These data have been compiled in a database managed by the ONF-RTM (http://rtm-onf.ifn.fr/). They show that the village of Ristolas (located 8 km downstream from Lake Foréant, Fig. 1C) has been affected at least 34 times over the last 250 years by floods of the Guil River and its five main tributaries (see Supplementary Material).

2.2. Lake Foréant and its tributaries

Lake Foréant (2620 m a.s.l., 44°42'20"N, 6°59'00”E) is located in a cirque of 3 km² in the upper part of the Queyras Massif, adjacent to the Italian border (Fig. 1). It is located approximately 60 km north from Lake Allos and 100 km south-west from Lakes Blanc, whose hydro-climatic settings are characterized by the south-western and north-western flood pattern, respectively (Wilhelm et al., 2012a,b; Fig. 1B). The catchment rises up to 3210 m. a.s.l. and is made up of three lithologies from the Queyras schistes-lustrés nappe (e.g. Schwartz et al., 2009); (i) marble in the eastern part, (ii) calc-schist in the western part and (iii) a narrow band of arkose in between (Fig. 1D). The main stream of the catchment, the Torrent de Bouchouse, drains mainly the central band of arkose. Before entering the lake, this stream has built an alluvial plain (Fig. 1E). This suggests that the Bouchouse stream is a major source of sediment entering the lake. In addition, two minor and non-permanent streams drain the western part of the catchment. In contrast, they enter the lake through only small deltas compared to the Bouchouse inflow area, suggesting limited detrital inputs. There is no evidence that the catchment was glaciated in the past, i.e. no moraine or other glacial deposits occur. Thereby, detrital inputs only result from the erosion and transport of these lithologies. Detrital inputs from these streams are limited to summer and fall because the catchment is covered by snow and the lake is frozen from mid-November to the beginning of June. The Bouchouse stream flows downstream into the Guil River and reaches approximately 8 km further the village of Ristolas (Fig. 1C).

3. Method

3.1. Lake coring

In summer 2013, a bathymetric survey was carried out on Lake Foréant and revealed a well-developed flat basin in the centre of the lake with a maximum water depth of 23.5 m (Fig. 1E). An UWITEC gravity corer was used to retrieve four cores along a north-south transect in the axis of the two main inlets of the Bouchouse stream. Cores FOR13P3 and FOR13P4 correspond to the proximal locations of the two different branches of the Bouchouse stream and aim at investigating their respective sediment inputs during floods. Cores FOR13P2 and FOR13P1 correspond to the depocenter and to the most distal position, i.e. the opposite slope to the Bouchouse inflows, respectively.

3.2. Core description and logging

Cores were split lengthwise and the visual macroscopic features of each core were examined to identify the different sedimentary lithofacies. The stratigraphic correlation between the cores was then carried out based on these defined lithofacies. The stratigraphic correlation allows identifying the depositional pattern of the event layers within the lake basin. Depositional patterns of event layers may help to decipher their trigger, i.e. mass-movements vs. flood events (e.g. Sturm and Matter, 1978; Wilhelm et al., 2012b; Van Daele et al., 2015).

High-resolution color line scans and gamma-ray attenuation bulk density measurements were carried out on a GeotekTM multisensor core-logger (Institute of Geological Sciences, University of Bern). Bulk density was used as a proxy of event layers, e.g. flood layers, characterized by higher density due to the high amount of detrital material (e.g. Støren et al., 2010; Gilli et al., 2012; Wilhelm et al., 2012b).

Geochemical analysis and X-ray imaging were carried out using an Itrax™ (Cox Analytical Systems) X-ray fluorescence (XRF) core scanner (Institute of Geological Sciences, University of Bern), equipped with a Molybdenum tube (50 keV, 30 mA) with a 10-s count-time using sampling steps of 1 mm (XRF) and 0.2 mm (X-ray imaging). Several studies could demonstrate that counts received from XRF core scanning are proportional to element concentrations if no important matrix effects due to pronounced lithology changes or

variations of pore water volume and chemical composition are present (e.g. Kylander et al., 2013; Russell et al., 2014). Geochemical data were applied to identify event layers at high resolution through their higher content in detrital material (e.g. Arnaud et al., 2012; Wilhelm et al., 2012b; Czymzik et al., 2013; Swierczynski et al., 2013) and/or as high-resolution grain-size analysis (e.g. Cuven et al., 2010; Wilhelm et al., 2012a; 2013). Geochemical analyses were carried out on core FOR13P2. X-ray images highlighting the variability of the sediment density have been acquired for the four cores.

Grain size analyses on core FOR13P2 were performed using a Malvern Mastersizer 2000 (Institute of Geography, University of Bern) on sub-samples collected at a 5-mm continuous interval. Before grain-size analysis, the samples were treated in a bath of diluted (30%) hydrogen peroxyde during 3 days to remove organic matter. After treatment, microscopic observations were performed to control that organic matter was totally dissolved. These grain-size analyses of the detrital material were performed to characterize event layers and, when event layers are induced by floods, to establish a proxy of flood intensity. Grain-size variability is assumed to be related with the stream flow energy of the river entering the lake and, thereby, with the peak discharge reached during the flood event (Campbell, 1998; Lapointe et al., 2012; Wilhelm et al., 2015). The flood intensity may also be reconstructed based on the amount of sediment transported and deposited during floods (e.g. Schiefer et al., 2011; Jenny et al., 2014; Wilhelm et al., 2015). This approach appears particularly relevant in case of an insignificant variability of the flood-sediment grain size (e.g. Jenny et al., 2014; Wilhelm et al., 2015). When the depositional pattern of the flood layers within the lake basin (assessed through the stratigraphic correlation) shows a high variability, many cores are required for a reliable assessment of the flood-sediment volumes (e.g. Page et al., 1994; Schiefer et al., 2011; Jenny et al., 2014). However, when the depositional pattern of the flood layers is stable over time, the layer thickness in one core may be sufficient (e.g. Wilhelm et al., 2012b; 2015). As a result, grain size and sediment volume of the event layers were both explored as two distinct proxies of flood intensity.

3.3. Coprophilous fungal spores analysis

Erosion processes in high-altitude catchments may be modified by grazing activity and, thereby, the climatic signal in flood reconstructions may be altered (e.g. Giguet-Covex et al., 2012). The variability of grazing intensity in a catchment area can be reconstructed from the

sedimentary abundance of coprophilous fungal ascospores, i.e. *Sporormiella* (HdV-113) (e.g. Davis and Schafer, 2006; Etienne et al., 2013). To test the potential impact of grazing intensity on the reconstructed flood activity, *Sporormiella* abundance was determined in subsamples collected all along the core FOR13P3 with an approximate step of 3 cm. This core was chosen because it was the sequence with the thinnest potentially-erosive event layers. During the sampling, event layers were avoided because they may correspond to layers induced by flood or mass-movement events that may have transported unusual quantities of *Sporormiella* ascospores, or induced the remobilization of older sediments. Subsamples were chemically prepared according to the procedure of Fægri and Iversen (1989). *Lycopodium clavatum* tablets were added in each subsample (Stockmarr, 1971) to express the results in concentrations (number.cm^{-3}) and accumulation rates (number.cm^2.yr^{-1}). Coprophilous fungal ascospores were identified based on several catalogues (Van Geel and Aptroot, 2006; Van Geel et al., 2003) and counted following the procedure established by Etienne and Jouffroy-Bapicot (2014).

3.4. Dating methods

For dating the lake sequence over the last century, short-lived radionuclides (^{210}Pb, ^{137}Cs) were measured by gamma spectrometry at the EAWAG (Zürich, Switzerland). The core FOR13P4 was sampled following a non-regular step of 1±0.2 cm. The non-regular step aims at matching the facies (i.e. sedimentary background or event layer) boundaries for homogeneous samples. The ^{137}Cs measurements allowed two main chronostratigraphic markers to be located: the fallout of ^{137}Cs from atmospheric nuclear weapon tests culminating in AD 1963 and the fallout of ^{137}Cs from the Chernobyl accident in AD 1986 (Appleby, 1991). The decrease in excess ^{210}Pb and the Constant Flux/Constant Sedimentation (CFCS) allowed a mean sedimentation rate to be calculated (Goldberg, 1963). The standard error of the linear regression of the CFCS model was used to estimate the uncertainty of the sedimentation rate obtained by this method. The ^{137}Cs chronostratigraphic markers are then used to control the validity of the ^{210}Pb-based sedimentation rate.

To date the sequence beyond the last century, small-size vegetal macro-remains were sampled in core FOR13P4. Terrestrial plant remains were isolated at the Institute of Plant Sciences (University of Bern) and sent for AMS ^{14}C analysis to the AMS LARA Laboratory (University of Bern). ^{14}C ages were calibrated using the Intcal13 calibration curve (Reimer et

al., 2013; Table 1). In addition, palaeomagnetic chronostratigraphic markers were also used. These markers can be obtained by comparing the characteristic declination and inclination of remanent magnetization (ChRM) versus depth to global geomagnetic models or to known secular variations of the geomagnetic field (e.g. Barletta et al., 2010; Wilhelm et al., 2012a). Palaeomagnetic investigations were performed at the CEREGE laboratory (University Aix-Marseille) and are detailed in supplementary material.

Using the R-code package "clam" (Blaauw, 2010), an age-depth model was generated from the ^{210}Pb ages, the ^{14}C ages and the palaeomagnetic chronological markers.

4. Results

4.1. Sedimentology

The sediment consists of a homogeneous, brown mud mainly composed of silty detrital material and aquatic organic remains (small fragments of plants and anamorphous organic matter), representing the background hemi-pelagic sedimentation. These fine grained deposits are interrupted by 171 rather coarser-grained layers, which are interpreted to represent short-term depositional events, i.e. event layers (Fig. 2).

The 171 event layers correspond to graded layers, characterized by their higher density, a slight fining-upward trend and a thin, whitish fine-grained capping layer (Fig. 2). There is no evidence of an erosive base. According to the stratigraphic correlation, almost all these graded layers (168 out of 171) extend over the entire lake basin with a regular deposition pattern. The thickness of these 168 graded layers is systematically larger in cores FOR13P2 and FOR13P4, and decreases respectively in cores FOR13P1 and FOR13P3. This suggests that the southern branch of the Bouchouse stream is the main sediment input over the studied period (Fig. 1). The grain-size of these graded layers is dominated by silt-sized grains with only small amounts of clay / fine silt present in the whitish capping layer and to coarse silt in their basal part (Fig. 2 and S1). The origin of these 168 is discussed in section 5.1. The three other graded layers show a higher variability in thickness, grain size and depositional pattern. Above all, they overlie three cm-thick coarse-grained layers, present at 75 cm in core FOR13P2 and at 9 and 42 cm in core FOR13P4 (Fig. 2). The coarse-grained layers consist of pebble gravels and aquatic plant remains embedded in a silty matrix. The high porosity in the sediment due to the presence of gravels generates a partial loss of XRF signal, preventing a

reliable geochemical characterization. X-ray images show chaotic sedimentary structures. The stratigraphic correlation revealed that two centimetres of sediment are missing below the thickest coarse-grained layer in core FOR13P4, suggesting an erosive base for this layer. The stratigraphic succession of a coarse-grained layer overlain by a graded layer (labelled MMIL in Fig. 2 and 3) suggests that the two layers were induced by a single event. Their origin is discussed in section 5.1.

4.2. Geochemistry

Among the core scanner output parameters, the scattered incoherent (Compton) radiation of the X-ray tube (Mo_{inc}) may vary with the sediment density (Croudace et al., 2006) and, thereby, offer a high-resolution proxy for sediment density. Mo_{inc} values were averaged at a 5-mm resolution to be compared to the density obtained at a 5-mm resolution with the gamma-ray attenuation method. A positive and significant correlation ($r=0.85$, $p<10^{-4}$) between the two density parameters was found and allowed using Mo_{inc} as a proxy of sediment density for identifying millimetre-scale event layers (Fig. 3).

The variability of other elements within the event layers was then investigated to assess i) a high-resolution grain-size proxy and ii) distinct sediment sources of the event layers between the littoral (i.e. mass-movement origin) and the catchment area (i.e. flood origin). The variability of potassium (K) intensities *vs.* sediment depth (Fig. 2 and S1) shows increased K intensities in the capping layers of the event layers, suggesting K enrichment in the finest sediment fraction. Variability in silicon (Si) intensities is correlated to K intensities ($r=0.77$, $p<10^{-4}$). Variations in iron (Fe) intensities show an opposite pattern with Fe enrichments in the basal and coarser part of the graded beds. Interestingly, Fe is the only element which elevated in event layers. These results suggest that the Fe/K ratio may be used as a millimetre-scale proxy for relative grain-size distribution and hence for detecting millimetre-scale event layers. However, since grain-size variability is insignificant, the information that can be won from this proxy in regard to flood-intensity reconstruction is minor.

Ca intensities are most of the time very low (< 900 counts), except for several sharp peaks and two well-marked excursions (> 1200 counts) at 30 and 75 cm in core FOR13P2 (Fig. 3). These two well-marked excursions correspond to the two thickest graded layers (labelled MMIL2 and 3; Fig. 2). In addition, manganese (Mn) intensities also vary within a low value range (< 10^4 counts) interrupted by sharp, well-marked peaks (up to 4.10^4 counts). All those

Mn peaks are located at the base of the 168 graded layers (those that not overlain a coarse-grain layers). However not every base of graded layers corresponds to a Mn peak. To better assess the relationships between those elements, the Ca intensities were plotted against Fe, K and Mn intensities (Fig. 3). These plots clearly highlight two groups of deposits. The background sediments and the 168 graded layers (those labelled FIL in Fig. 3) are characterized by i) low Ca intensities and ii) a high variability in Mn intensities. The three graded layers labelled MMIL in figure 2 show a distinct geochemical pattern with (i) high Ca intensities regardless of Fe and K intensities and (ii) very low Mn intensities.

4.3. Chronology

The down-core ^{210}Pb excess profile for core FOR13P2 shows a continuous decrease to low values (~50 Bq.Kg^{-1}), punctuated by sharp excursions to low values for three layers (2-3.5 cm, 7.5-10.5 cm and 15-17 cm) corresponding to graded layers (Fig. 4A). In line with Arnaud et al. (2002), these values were excluded to build a corrected sedimentary record without event layers (Fig. 4B). The CFCS model (Goldberg, 1963), applied on the event-free ^{210}Pb excess profile, provides a mean sedimentation rate of 1.3 ± 0.1 mm.yr^{-1} (without the event layers). Ages derived from the CFCS model were transposed to the original sediment sequence to provide a continuous age-depth relationship (Fig. 4C). The event-free ^{137}Cs profile indicated two peaks at 3.5 cm and 5.5 cm (Fig. 4B), interpreted as the result of the Chernobyl accident in AD 1986 and the maximum fallout of the nuclear weapon tests in AD 1963. These independent chronological markers are in good agreement with the ^{210}Pb excess ages, supporting the age-depth model over the last century (Fig. 4C).

In order to evaluate the reliability and efficiency of the palaeomagnetic results several points need to be verified: i) the preservation of the sedimentary magnetic fabric, ii) the stability of magnetic mineralogy, and iii) the stability of the magnetic components. Results of Anisotropy of Magnetic Susceptibility for core FOR13P4 show a well preserved sedimentary fabric, i.e. Kmin inclination close to the vertical, except in the thickest event layers (labelled MMIL2 and MMIL3, Fig. 2) were the Kmin inclination is clearly deviated (Fig. S2). For the 3 cores, the mean destructive field of ARM and IRM is very similar (between 20 and 30 mT) indicating a magnetic mineralogy mainly composed of low coercivity phase. The S-ratio (Bloemendal et al., 1992) is always between 0,86 and 0,95 indicating lower coercivity and a ferrimagnetic mineralogy. This suggests a good stability of the magnetic mineralogy, except

in event layers where other parameters such as the relative palaeointensity (calculated as NRM intensity divided by ARM intensity) are clearly different, highlighting a different magnetic mineralogy. PCA have then been performed using puffin plot software (Lurcock and Wilson, 2012) to calculate the ChRM. A careful examination of demagnetization diagrams shows a unidirectional behaviour (Fig. S3). The Mean Angular Deviation (MAD) is usually lower than 6 revealing a good stability of the magnetization direction. In most cases, the calculated component is not straight to the origin. This is particularly the case in the event layers. This implies the occurrence of a high coercivity component of unknown origin. All cores show quite large variations of the declination and inclination *vs.* depth. Because of the deviation of the Kmin and changes in magnetic mineralogy, measurements from the thickest event layers (i.e. MMIT2 and MMIT3) have been removed to build event-free declination and inclination signals (Fig. 5A). Based on the stratigraphic correlation, the event-free palaeomagnetic profiles obtained for each core were all corrected to a reference depth, i.e. the event-free depth of core FOR13P2 (Fig. 5B). Finally, all magnetic profiles were averaged to obtain unique curves of declination *vs.* depth and inclination *vs.* depth (Fig. 5C), smoothing small artefacts and making it easier for comparison to the reference curve (ARCH3.4k model; Donadini et al., 2009; Korte et al., 2009). From the variations of the reference curve over the last millennium, magnetic declination minima and maxima can be identified at AD 1810 ±20, 1540 ±70 and 1365 ±25 (D-1 to D-3, respectively). For the inclination, two tie points at AD 1700 ±30 and 1330 ±40 can be used (I-1 and I-2, Fig. 5D). Furthermore the ChRM declination profile presents 3 declination features and the ChRM inclination profile presents 2 inclination features over this period, allowing the correlation proposed (Fig. 5). These well-correlated declination and inclination features can thus be used as additional chronological markers.

The ^{210}Pb and the ^{14}C ages (Fig. 4 and Table 1) were then combined with the palaeomagnetic chronomarkers (Fig. 5) to construct an age-depth model covering the whole sequence (Fig. 6). As noted above, the age-depth model was calculated on an event-free depth using a smooth spline with the “clam” R-code package (Blaauw, 2010). This revealed that the sequence FOR covers the last millennium with a mean sedimentation rate of 1 mm.yr^{-1} (without event layers).

5. Discussion

5.1. Different triggers for event layers

5.1.1. Mass movements

The unusual presence of gravel and aquatic plant remains, in combination with the chaotic sedimentary structures and the localized deposition areas, suggest that the coarse-grained layers result of a mass movement originating from sediment-charged slopes (e.g. Sauerbrey et al., 2013). The three graded layers overlying the coarse-grained layers are then resulting from the sediment that is transported in suspension during sliding of subaquatic slope sediments and then deposited over the coarse-grained layers and further into the lake basin (e.g. Girardclos et al., 2007; Moernaut et al., 2014). As a result, each stratigraphic succession of a graded and a coarse-grained layer is interpreted as a mass-movement-induced layer (MMIL). These MMILs are well characterized by higher Ca intensities that suggest a distinctly different sediment source when compared to the sedimentary background and to the 168 graded layers that not overlain a coarse-grain layer. The coarse-grained layer of MMIL3 is only present in core FOR13P3, suggesting a littoral origin of the mass movement (Fig. 2). The two coarse-grained layers of MMIL1 and MMIL2 are located in core FOR13P4 (Fig. 2). These layers may thus originate either from the delta or from the littoral slopes. Slope angles of < 10° and ~15° for delta and littoral slopes of Lake Foréant, respectively, point to a littoral origin as suggested by many studies showing that slope angles > 10° are favourable for the generation of mass-movements (e.g. Moernaut et al., 2007; Strasser et al., 2011; Van Daele et al., 2013). In addition, higher Ca intensities are often an indicator of littoral sediments as a result of increased fluxes of endogenic calcite when compared to the open-water endogenic production.

5.1.2. Flood events

The 168 graded layers may be induced by either mass movements or flood events (e.g. Sturm and Matter, 1978). Their extents over the whole basin with a relatively homogeneous deposition pattern, their frequent occurrence and a different geochemical pattern suggest a distinct origin from that of the MMIL graded layers. The low Ca intensities suggest a minor

sediment contribution of the marble and calc-schists in favour of a major contribution of the arkose band, which is the lithology drained by the main inflow (Fig. 1). The 168 graded layers are also characterized by sharp peaks of Mn only located at their bases. This location suggests that the punctual enrichement in Mn is related to the occurrence of these event layers. Mn is a redox sensitive element and more soluble under reducing conditions (e.g. Davison, 1993; Torres et al., 2014). The punctual presence of detectable Mn at the base of the graded layers suggests that hyperpycnal turbidity currents carry oxygen to the deeper parts of the basin. Dissolved oxygen is probably also trapped in pore waters of the individual graded layers. Based on these considerations we suggest that dissolved and reduced Mn is, in part due to the rapid increase in loading from the graded layers, migrating from pore waters of the buried sediments into oxygenated graded layers where it is oxidized and precipitated likely in form of an Mn-oxyhydroxide (e.g. Davison, 1993; Deflandre et al., 2002). The fast sediment deposition during the event-layer formation and the low reactive organic matter concentrations would then prevent reductive dissolution of the Mn-oxyhydrxide precipitates (e.g. Torres et al., 2014). According to these layer characteristics, flood events are the most probable candidate to trigger the 168 graded layers because i) these events may be frequent (e.g. Czymzik et al., 2013), ii) these events may bring both high oxgygen and detrital inputs in a short time (e.g. Deflandre et al., 2002), and iii) the nature of the sediment correspond the most to the main lithology drained by the inflow. Hence, the 168 graded layers likely correspond to flood-induced layers (FIL).

5.1.3. Chronological controls

MMILs can be triggered by spontaneous failures due to overloading/oversteepening of sediments-charged slopes, snow avalanches, rockfalls, earthquakes or fluctuations in lake levels (e.g. Monecke et al., 2004; Girardclos et al., 2007; Moernaut et al., 2014). In case of Lake Foréant, changes in lake level can be excluded because water levels of Lake Foréant are well controlled by bedrock outlets. In addition, there is no geomorphological evidence of major rockfalls in the catchment area. Regarding earthquakes, many events occurred in the region and affected the population and infrastructure. Historical earthquakes are well documented thanks to the database SisFrance (http://www.sisfrance.net, Lambert and Levret-Albaret, 1996; Scotti et al., 2004). An earthquake trigger for the MMILs can then be investigated by comparing ages of the MMILs to the dates of the closest and/or strongest historical earthquakes (e.g. Avşar et al., 2014; Howarth et al., 2014). The three MMILs are

respectively dated to AD 1963 (±6), AD 1814 (+50/-39) and AD 1456 (+19/-56) (Fig. 6). The age of the most recent deposit is consistent with the Saint-Paul-sur-Ubaye earthquake (AD 1959), characterized by an epicentre at ca. 20 km from the lake where the MSK intensity reached VII-VIII. The age of the second deposit is consistent with the Piemont (Torre Pellice) earthquake (AD 1808), characterized by an epicentre at ca. 20 km from the lake and a MSK intensity of VIII (Fig. 6). For the older period of the third deposit, data of documented earthquakes are sparser in the catalogue, precluding a reliable assignment. The earthquakes of Saint-Paul-sur-Ubaye and Piemont are both the closest and strongest historically-known earthquakes around the lake, suggesting that they are the most probable trigger of the temporarily corresponding subaquatic landslides. Overall, there is a good agreement between major historical events and the calculated ages of the MMILs supporting their sedimentologic interpretation and the chronology over the last centuries.

5.2. Palaeoflood record

A flood chronicle of the Bouchouse stream was built by dating the 168 FILs over the last millennium. Changes in flood frequency are highlighted through a running sum of flood occurrences with an 11-year (Fig. 7) or 31-year window (Fig. 8). The absence of significant grain-size variability precludes the use of grain size to assess changes in flood intensity (e.g. Giguet-Covex et al., 2012; Lapointe et al. 2012; Wilhelm et al., 2013, 2015). The relatively homogeneous grain size of the FILs makes the sediment accumulation per event a more suitable proxy of flood intensity (e.g. Jenny et al., 2014). In addition, the relatively homogeneous flood-sediment deposition pattern within the lake basin makes it possible to use the FIL thickness as a proxy of the flood-sediment accumulation as shown by previous calibration in Alpine environments (Wilhelm et al., 2012b; Jenny et al., 2014; Wilhelm et al., 2015). Hence, the FIL thickness is here assumed to represent the flood intensity, under the condition that erosion processes and availability of erodible materials in the catchment did not change significantly over time.

5.2.1. Proxy validation

To control the reliability of our reconstruction, the Foréant palaeoflood record is compared to the historical floods at Ristolas located around 8 km downstream the lake (Fig. 1C and Supplementary Material). The almost absence of documented flood event for the Bouchouse

stream (outlet of Lake Foréant) precludes an event-to-event comparison as undertaken with the Lake Allos record (Wilhelm et al., 2015). Hence, the 21 flood events having affected the village of Ristolas and occurring during the ice-free season of the lake (mid-June to mid-November) have been considered to reconstruct a historical flood record (Fig. 7). This includes 6 floods considered as 'local' because they only affected the village of Ristolas (catchment area of ca. 80 km²) and 15 floods considered as 'sub-regional' because they also affected other villages downstream (Abriès, Aiguilles, Chateau-Vieille-Ville, catchment area of ~320 km²). Through comparison of the historical chronicles and the lake records, we observe that the ranges of flood-frequency values are similar, i.e. between 0 and around 4 floods per 11 years. We also observe strong similarities in the two flood records with common periods of low flood frequency in AD 1750-1785, 1820-1860 and 1910-1945 and common periods of high flood frequency in AD 1785-1820, AD 1945-1970 and AD 1985-2000. Only a slight time lag (~5 years) appears for the latter period in the lake record. Overall, there is then good agreement with the historical data, supporting that Lake Foréant sediments record the variability of past flood events that impacted societies over the last 250 years relatively well. A major inconsistency, however, appears from 1860 to 1910 since numerous floods are documented in the lake record but there is missing evidence for flood in the historical record. A high hydrological activity is documented for the region at this time (e.g. Miramont et al., 1998; Sivan et al., 2010; Wilhelm et al., 2012a; 2015), suggesting that this may result of a historical database locally incomplete.

5.2.2. Potential influences of environmental changes

The Foréant flood record may be considered as relevant over the entire studied period if erosion processes are stable over time. Erosion processes in the Foréant catchment may be affected by modifications in the river system and/or by land-use changes.

The main inflow, the Bouchouse stream, has built an alluvial plain upstream the lake where it is divided in two main meandering branches. An alternate activity of these branches during floods may disturb the flood record by triggering variable sediment dispersion within the lake basin (e.g. Wilhelm et al., 2015). However, such processes seem to be unlikely because the stratigraphic correlation highlights a stable pattern of the flood-sediment deposition with the thickest FILs in cores FOR13P2 and FOR13P4 from the depocenter and a thinning of the FIL deposits toward cores FOR13P1 and FOR13P3 located in the slopes (Fig. 2). The alluvial

plain may also disturb the record by acting as a sediment trap. Indeed, the meandering river morphology and the gentle slope of the alluvial plain may trigger a decrease of the discharge velocity, resulting in the deposition of the coarser particles on the plain before entering the lake. This may explain the small variability in grain-size in the Foréant sediment record. The grain-size ratio between the base (coarser fraction) and the top (finer fraction) of the FILs is ~1.3, while it usually ranges from 5 to 15 in many different geological and environmental settings (e.g. Oslegger et al., 2009; Giguet-Covex et al., 2012; Simmoneau et al., 2013; Wilhelm et al., 2013 Amman et al., 2015; Wilhelm et al., 2015). However, fine particles (i.e. clays and fine silts that composed the FILs) are transported by suspension in the river (e.g. Passega, 1964). As a result, their trapping and storage in the alluvial plain is unlikely. A negligible storage effect on the fine fraction is also supported by the relatively stable sedimentation rate of the silty sedimentary background (Fig. 6) that suggests an uninterrupted sediment transport to the lake over the studied period.

Erosion processes in the catchment may also be modified by land-use that mainly corresponds at this altitude to changes in grazing intensity. An increase of grazing intensity may make soils more vulnerable to erosion during heavy rainfalls and, thereby, may induce an increased sensitivity of the catchment-lake system to record floods, i.e. higher flood frequency and/or flood-sediment accumulation in the sediment record (e.g. Giguet-Covex et al., 2012). Abundance of *Sporormiella* is assumed to reflect local changes of grazing intensity in Lake Foréant catchment (e.g. Etienne et al., 2013). The concentration of *Sporormiella* ascospores measured in core FOR13P3 oscillated from 5 to 43 number.cm^{-3} through the sequence (Fig. 2), resulting in accumulation rates varying from 12 to 340 number.cm².yr^{-1} over time (Fig. 8). This variability in *Sporormiella* abundance has been compared to the variability in flood frequency and flood-sediment accumulation (see Supplementary Material). We do not find significant relationships ($p > 0.05$) between these parameters (Fig. S4), suggesting that variations in pastoralism seemingly have not had a significant impact on erosion processes in the Foréant catchment. However, two samples covering the period AD 1734-1760 show both high *Sporormiella* accumulation rates and flood frequencies (Fig. 8 and S3). This suggests that the flood frequency during this period may be exacerbated by a punctual and very high grazing intensity. Hence, we postulate that erosion processes did not change drastically over the studied period, implying that climate is likely the main factor explaining the recorded flood activity, with exception of the period AD 1734-1760.

5.2.3. Palaeoflood activity in the regional climatic setting

Comparison with the historical record shows that the past flood variability is well reproduced by the Foréant record (Fig. 7). The Foréant palaeoflood record is thus interpreted as the recurrence of summer-to-autumn flood events triggered by both local and mesoscale convective phenomena.

To discuss the millennium-long flood variability in regard to both Atlantic and Mediterranean climatic influences in the Alpine domain, the Foréant palaeoflood record is compared to the palaeoflood records of Lakes Blanc and Allos (Fig. 7 and 8). Lakes Blanc and Allos have similar characteristics to Lake Foréant such as the high altitude (> 2000 m a.s.l.), the small catchment area (< 3 km²) and the steep catchment slopes, making possible the comparison. Lake Blanc sediments located in the northern French Alps mainly record Atlantic-sourced weather pattern of high altitude, i.e. summer local convective events (Fig. 1; Giguet-Covex et al., 2012; Wilhelm et al., 2012b, 2013). In contrast, Lake Allos sediments located in the southern French Alps mainly record Mediterranean-sourced weather patterns of high altitude, i.e. mesoscale convective events (Fig. 1; Wilhelm et al., 2012a, 2015). The last millennium is usually divided in three climatic periods according to the temperature variations; the warm Medieval Climate Anomaly (MCA, ca. AD 950-1250), the cold Little Ice Age (LIA, ca. AD 1300-1900) and the warmer 20th century (e.g. Lamb, 1965; Büntgen et al., 2011; Luterbacher et al., 2012 and references therein). During the MCA, the Foréant flood record shows a low flood frequency with ~10 floods per century and, 4 occurrences of thick flood deposits (> 8 mm thick) that we interpret as high-intensity flood events. During the LIA, the Foréant record shows a higher flood frequency with ~17 floods per century and only 2 high-intensity events. The 20th century is finally characterized by ~17 floods per century and absence of high-intensity events. The increased flood frequency during the long and cold period of the LIA, compared to the MCA, was also observed in the Blanc and Allos records (Wilhelm et al., 2012a; 2013; Fig. 8), as well as in many other records from the European Alps (e.g. Arnaud et al., 2012; Glur et al., 2013; Swierczynski et al., 2013; Wirth et al., 2013a, 2013b; Amann et al., 2015; Schulte et al., 2015) and the north-western Mediterranean area (e.g. Jorda and Provansal, 1996; Camuffo and Enzi, 1995; Jorda et al., 2002; Thorndycraft and Benito, 2006; Moreno et al., 2008; Benito et al., 2015; Arnaud-Fassetta et al., 2010). This common pattern in many flood records of southern Europe may be the result of a southward shift and an intensification of the dominant westerly winds during boreal summer related to an increase in the thermal gradient between low (warming) and high (cooling) latitudes (e.g. Bengtsson and

Hodges, 2006; Raible et al., 2007). In this scenario, the Alps are likely to experience an increase in precipitation due to an increase in moisture advection from the North Atlantic. In contrary, the occurrence of high-intense floods during both the MCA and the LIA periods is a new feature of Alpine regional patterns, since the most intense floods occurred exclusively during the MCA in the Blanc record (Wilhelm et al., 2013) or during the LIA in the Allos record (Wilhelm et al., 2012a; Fig. 8) and other Mediterranean records of the Alpine region (Jorda and Provansal, 1996; Miramont et al., 1998; Jorda et al., 2002; Arnaud-Fassetta et al., 2010). This suggests that hydro-meteorological processes related to the Atlantic and to the Mediterranean climatic influences may alternatively trigger high intense events in the Foréant area during the MCA and the LIA, respectively. However, the most intense floods at Foréant appear 3 times more frequent during the MCA than during the LIA, a trend that remains true when considering various thickness thresholds (8, 7, 6 or 5 mm) for high-intensity flood events. In addition, the mean sediment accumulation per flood event shows values ~50% higher during the MCA than during the LIA (3.8 *vs.* 2.4 mm/flood), suggesting an increase of the mean flood-event intensity during the warmer period. These two evidences of increased flood intensity during the warm period may be related to the strengthening of local convective processes due to higher temperatures, as suggested for the north-western flood pattern (Giguet-Covex et al., 2012; Wilhelm et al., 2012b, 2013). In the Foréant area, higher temperatures seem thus to result in a lower flood frequency but in higher flood intensity on the multi-centennial time scale. Flood frequency and intensity during the warmer 20th century, however, do not follow these trends. The frequency is still similar to the LIA one and high-intense events are absent and the mean sediment accumulation per flood event (2.2 mm/flood) is also similar to the LIA. Two hypotheses may be considered to explain this ‘anomaly’. First, this may result from the relatively short period covered by the 20th century (i.e. ~100 years) in comparison with the multi-centennial variability documented for the MCA (i.e. ~300 years) and the LIA (i.e. ~600 years) periods. Thereby, considering stable temperature-flood relationships over time, the 20th century might be a transitional period toward a MCA-like flood pattern with the global warming. This latter possibility would imply an increasing flood hazard in the Foréant region in a near future due to an increased occurrence of high-intensity flood events. Secondly, this may also result from a non-linearity of the flood response to temperature, making the analogy between the MCA and the 20th century more complex, in particular as the current warming is caused by an unprecedented forcing (greenhouse gases). Moreover, the other external forcing such as solar activity, and volcanic eruptions largely varied over the last millennium (e.g. Servonnat et al., 2010; Delaygue et Bard, 2011; Gao et

al., 2012; Crowley and Unterman, 2013) and their non-linear combination also with the greenhouse gases may result in different time-space temperature patterns and, thereby, in different flood responses during these two periods. In order to explore forcing-dependent impacts on the climate-flood relationships, deeper analysis utilizing for example advanced statistics or simulations is required.

6. Conclusion

High-resolution sedimentological and geochemical analyses of the Lake Foréant sequence revealed 171 event layers. Three of the 171 event layers can be differentiated by characteristic geochemical features (high Ca contents and low Mn contents) and stratigraphic succession. These three event layers are interpreted as mass-movement-induced layers. The other 168 event layers show a geochemical pattern similar to the sedimentary background that mainly corresponds to detrital material sourced by the rivers. These event layers are interpreted as flood-induced layers. Only small changes in grain-size variability in the flood-induced layers precluded the use of the grain size as a flood-intensity proxy. However, the relatively homogeneous grain size and deposition pattern within the lake basin made the flood-deposit thickness a suitable proxy for the reconstruction of flood intensity.

Comparison with local historical data indicates that Foréant sediments sensitively record past flood events with variability in frequency and intensity related to both Atlantic- and Mediterranean-influenced hydro-meteorological processes, i.e. local and mesoscale convective systems occurring from late spring to fall. As there is no evidence of major changes in erosion processes due to landscape evolution or grazing intensity (except maybe for the period AD 1734-1760), we assume that climate and not land-use changes exerts the dominant control on flood variability in the Foréant-record over the past millennium. The comparison to northern and southern flood records, i.e. to Atlantic- and Mediterranean-influenced records, highlights that the increase of flood frequency during the cold period of the LIA is a common feature of all regional flood patterns from the European Alps. The comparison also revealed that high-intensity events in the Foréant region occurred during both the cold LIA and the warm MCA periods. This specific feature of the Foréant flood record likely results from its sensitivity to both Atlantic and Mediterranean climatic influences. However, high-intensity events are more frequent and the flood intensity is higher during the warm MCA. This suggests that flood hazard may increase in the Foréant region in response to

global warming. Surprisingly, the flood variability over the warm 20th century appears still similar to the flood variability of the cold LIA period. This 20th-century flood trend may be interpreted as the result of a transitional period toward a MCA-like flood pattern. This would imply an increasing flood hazard in the Foréant region in a near future due to more frequent high-intensity flood events. However, this may also result from a non-linear temperature-flood relationship. In order to better understand the underlying mechanisms deeper analyses employing advanced statistics or simulations need to be applied.

Acknowledgments

B. Wilhelm's post-doctoral fellowship (2013-2014) was supported by a grant from the AXA Research Fund. We would also like to thank Pierre Sabatier for his help with analysis of the ^{210}Pb data, Anne-Lise Develle for fruitful discussions, Petra Boltshauser-Kaltenrieder for help with identification of terrestrial-plant remains prior to ^{14}C dating and Nicolas Thouveny and François Demory for providing access to facilities at the CEREGE palaeomagnetic laboratory (Aix-Marseille University) and for fruitful discussions.

References

Amann, B., Sönke, S., Grosjean, M.: A millennial-long record of warm season precipitation and flood frequency for the North-western Alps inferred from varved lake sediments: implications for the future, Quaternary Science Reviews, 115, 89-100, 2015.

Appleby, P.G., Richardson, N., Nolan, P.J.: 241Am dating of lake sediments, Hydrobiologia, 214, 35–42, 1991.

Arnaud, F., Lignier, V., Revel, M., Desmet, M., Pourchet, M., Beck, C., Charlet, F., Trentesaux, A., Tribovillard, N.: Flood and earthquake disturbance of 210Pb geochronology (Lake Anterne, North French Alps), Terra Nova, 14, 225–232, 2002.

Arnaud, F., Révillon, S., Debret, M., Revel, M., Chapron, E., Jacob, J., Giguex-Covex, C., Poulenard, J., Magny, M.: Lake Bourget regional erosion patterns reconstruction reveals

641 Holocene NW European Alps soil evolution and paleohydrology, Quaternary Science
642 Reviews, 51, 81–92, 2012.

643 Arnaud-Fassetta, G., and Fort, M.: Respective parts of hydroclimatic and anthropic factors in
644 the recent eveolution (1956-2000) of the active channel of the Upper Guil, Queyras, Southern
645 French Alps, Méditerranée, 102, 143-156, 2004.

646 Arnaud-Fassetta, G., Carcaud, N., Castanet, C. and Salvador, P.G.: Fluviatile
647 palaeoenvironments in archaeological context: geographical position, methodological
648 approach and global change—hydrological risk issues, Quat. Int., 216, 93–117, 2010.

649 Avşar, U., Hubert-Ferrari, A., De Batist, M., Lepoint, G., Schmidt S. and Fagel N.:
650 Seismically-triggered organic-rich layers in recent sediments from Göllüköy Lake (North
651 Anatolian Fault, Turkey), Quat. Sci. Rev., 103, 67–80, 2014.

652 Barletta, F., St-Onge, G., Channell, J.E.T. and Rochon, A.: Dating of Holocene western
653 Canadian Arctic sediments by matching paleomagnetic secular variation to a geomagnetic
654 field model, Quaternary Science Reviews, 29, 2315–2324, 2010.

655 Bengtsson, L., and Hodges, K.I.: Storm tracks and climate change, Journal of Climate, 19,
656 3518–3543, 2006.

657 Beniston, M. and Stephenson, D.B.: Extreme climatic events and their evolution under
658 changing climatic conditions, Glob Planet Change, 44, 1–9, 2004.

659 Benito, G., Macklin, M.G., Zielhofer, C., Jones A., and Machado, M.J.: Holocene flooding
660 and climate change in the Mediterranean, Catena, 130, 13-33, 2015.

661 Blaauw, M.: Methods and code for 'classical' age modelling of radiocarbon sequences, Quat.
662 Geochronol., 5, 512–518, 2010.

663 Bloemendal, J., King, J.W., Hall, F.R. and Doh, S.-J.: Rock magnetism of Late Neogene and
664 Pleistocene deep-sea sediments relationship to sediment source, diagenetic processes, and
665 sediment lithology, Journal of Geophysical Research, 97: 4361-4375, 1992.

666 Boudevillain, B., Argence, S., Claud, C., Ducrocq, V., Joly, B., Lambert, D., Nuissier, O.,
667 Plu, M., Ricard, D., Arbogast, P., Berne, A., Chaboureau, J.P., Chapon, B., Crepin, F.,
668 Delrieu, G., Doerflinger, E., Funatsu, B.M., Kirstetter, P.E., Masson, F., Maynard, K.,
669 Richard, E., Sanchez, E., Terray, L. and Walfpersdorf, A.: Cyclogeneses et precipitations
670 intenses en region mediterraneenne: origines et caracteristiques, La Meteorol., 66, 18–28,
671 2009.

672 Boroneant, C., Plaut, G., Giorgi, F. and Bi., X.: Extreme precipitation over the Maritime Alps
673 and associated weather regimes simulated by a regional climate model: Present-day and future
674 climate scenarios, Theor. Appl. Climatol., 86, 81–99, 2006.

675 Büntgen, U., Tegel, W., Nicolussi, K., McCormick, M., Frank, D., Trouet, V., Kaplan, J.,
676 Herzig, F., Heussner, U., Wanner, H., Luterbacher, J., Esper, J. : 2500 years of European
677 climate variability and human susceptibility, Science, 331, 578-582, 2011

678 Buzzi, A. and Foschini, L.: Mesoscale meteorological features associated with heavy
679 precipitation in the Southern Alpine Region, Meteorol. Atmos. Phys., 72, 131–146, 2000.

680 Campbell, C.: Late Holocene lake sedimentology and climate change in southern Alberta,
681 Canada, Quatern. Res., 49, 96–101, 1998.

682 Camuffo, D. and Enzi, S.: The analysis of two bi-millenary series: Tiber and Po River Floods,
683 In: Jones, P.D. Bradley, R.S. Jouzel, J. (Eds.), Climatic Variations and Forcing Mechanisms
684 of the Last 2000 years, NATO ASI Series, Series I: Global Environmental Change, 41
685 Springer, Stuttgart, 433–450, 1995.

686 Corella, J.P., Benito, G., Rodriguez-Lloveras, X., Brauer, A. and Valero-Garcès, B.L.:
687 Annually-resolved lake record of extreme hydro-meteorological events since AD 1347 in NE
688 Iberian Peninsula, Quat. Sci. Rev., 93, 77-90, 2014.

689 Croudace, I.W., Rindby, A. and Rothwell, R.G.: ITRAX: description and evaluation of a new
690 multi-function X-ray core scanner. In: Rothwell, R.G. (Ed.), New Techniques in Sediment
691 Core Analysis, Geological Society, London, Special Publications, 367, 51-63, 2006.

692 Crowley, T.J. and Untermann, M.B.: Technical details concerning development of a 1200-yr
693 proxy index for global volcanism, Earth Syst. Sci. Data, 5, 187-197, 2013.

694 Cuven, S., Francus, P. and Lamoureux, S.: Estimation of grain size variability with micro X-
695 ray fluorescence in laminated lacustrine sediments, Cape Bounty, Canadian High Arctic,
696 Journal of Paleolimnology, 44, 803–817, 2010.

697 Czymzik, M., Brauer, A., Dulski, P., Plessen, B., Naumann, R., von Grafenstein, U. and
698 Scheffler, R.: Orbital and solar forcing of shifts in Mid- to Late Holocene flood intensity from
699 varved sediments of pre-alpine Lake Ammersee (southern Germany), Quatern. Sci. Rev., 61,
700 96–110, 2013.

701 Davis, O.K. and Schafer, D.: *Sporormiella* fungal spores, a palynological means of detecting
702 herbivore density. Palaeogeo., Palaeoclimatol., Palaeoecol., 237, 40–50, 2006.

Davison, W.: Iron and manganese in lakes, Earth-Science Reviews, 34, 119-163,1993

Deflandre, B., Mucci, A., Gagne, J.P., Guignard, C., Sundby, B.: Early diagenetic processes in coastal marine sediments disturbed by a catastrophic sedimentation event, Geochimica et Cosmochimica Acta, 66(14), 2547–2558, 2002.

Delaygue, G. and Bard, E.: An Antarctic view of Beryllium-10 and solar activity for the past millennium, Climate Dynamics, 36, 2201–2218, 2011.

Donadini, F., M. Korte, Constable C. G.: Geomagnetic field for 0–3 ka: 1. New data sets for global modeling, Geochemistry Geophysics Geosystems (G3), 10, Q06007, doi:10.1029/2008GC002295, 2009.

Durant, Y., Laternser, M., Giraud, G., Etchevers, P., Lesaffre, B., Merindol, L.: Reanalysis of 44 Yr of Climate in the French Alps (1958–2002): Methodology, Model Validation, Climatology, and Trends for Air Temperature and Precipitation, J. Applied Meteorology and Climatology, 48(3):429-449, 2009.

Etienne, D., Wilhelm, B., Sabatier, P., Reyss, J.L. and Arnaud, F.: Influence of sample location and livestock numbers on *Sporormiella* concentrations and accumulation rates in surface sediments of Lake Allos, French Alps, J. Paleolimnol., 49, 117–127, 2013.

Etienne, D. and Jouffroy-Bapicot, I.: Optimal counting limit for fungal spore abundance estimation using *Sporormiella* as a case study. Veget. Hist. Archaeobot, 23, 743-749, 2014.

Faegri, K. and Iversen, J.: Textbook of Pollen Analysis. John Wiley & Sons, New York. 328, 1989.

Frei, C., Schöll, R., Fukutome, S., Schmidli, J., Vidale, P.L.: Future change of precipitation extremes in Europe: Intercomparison of scenarios from regional climate models, J. Geophys. Res. Atm., 111, D06105. doi:10.1029/2005JD005965, 2006.

Gao, C., Robock, A. and Ammann, C.: Volcanic forcing of climate over the past 1500 years: An improved ice core-based index for climate models, J. Geophys. Res., 113, D23111, 2008.

Giguet-Covex, C., Arnaud, F., Enters, D., Poulenard, J., Millet, L., Francus, P., David, F., Rey, P.J., Wilhelm, B. and Delannoy, J.J.: Frequency and intensity of high altitude floods over the last 3.5 ka in NW European Alps, Quatern. Res., 77, 12–22, 2012.

Gilli, A., Anselmetti, F.S., Glur, L. and Wirth, S.B.: Lake sediments as archives of recurrence rates and intensities of past flood events, In: Dating Torrential Processes on Fans and Cones –

Methods and Their Application for Hazard and Risk Assessment (Eds M. Schneuwly-Bollschweiler, M. Stoffel and F. Rudolf-Miklau), Adv. Global Change Res. 47, 225–242, 2012.

Girardclos, S., Schmidt, O.T., Sturm, M. , Ariztegui, D., Pugin A., and Anselmetti F.S.: The 1996 AD delta collapse and large turbidite in Lake Brienz, Marine Geology, 24, 137–154, 2007.

Glur, L., Wirth, S.B., B€untgen, U., Gilli, A., Haug, G.H., Schär, C., Beer, J. and Anselmetti, F.S., Frequent floods in the European Alps coincide with cooler periods of the past 2500 years, Sci. Rep., 3, 2770, 2013.

Goldberg, E.D.: Geochronology with 210Pb Radioactive Dating, IAEA, Vienna, 121–131. 1963

Gottardi, F., Obled, C., Gailhard, J., Paquet, E.: Statistical reanalysis of precipitation fields based on ground network data and weather patterns: Application over French mountains, J. Hydrology, 432–433, 154–167, 2010.

Howarth, J.D., Fitzsimons, S.J., Norris, R.J. and Jacobsen, G.E.: Lake sediments record high intensity shaking that provides insight into the location and rupture length of large earthquakes on the Alpine Fault, New Zealand, Earth and Planetary Science Letters, 403, 340–351, 2014.

IPCC: The Physical Science Basis. Contribution of Working Group I to the Fifth Assessment Report of the Intergovernmental Panel on Climate Change (Eds T.F. Stocker, D. Qin, G.-K. Plattner, M. Tignor, S.K. Allen, J. Boschung, A. Nauels, Y. Xia, V. Bex and P.M. Midgley). Cambridge University Press, Cambridge, United Kingdom and New York, NY, USA, 2013

Jorda, M. and Provansal, M.: Impact de l’anthropisation et du climat sur le detritisme en France du sud-est (Alpes du Sud et Provence), Bulletin de la Societe Geologique de France, 167, 159–168 ,1996.

Jorda, M., Miramont, C., Rosique, T. and Sivan, O.: Evolution de l’hydrosysteme durancien

(Alpes du Sud, France) depuis la fin du Pleniglaciaire superieur, In: Bravard, J.-P., Magny, M. (Eds.), Les Fleuves ont une Histoire, Paleo-environnement des Rivieres et des lacs Francais depuis 15000 ans. Errance, Paris, 239–249, 2002.

Jenny, J.-P., Wilhelm, B., Arnaud, F., Sabatier, P., Giguet-Covex, C., Mélo, A., Fanget, B., Malet, E., Ployon, E. and Perga, M.E., A 4D sedimentological approach to reconstructing the

764 flood frequency and intensity of the Rhône River (Lake Bourget, NW European Alps), J.
765 Paleolimnol., 51, 469–483, 2014.

766 Kylander, M.E., Klaminder, J., Wohlfarth, B., Löwemark, L.: Geochemical responses to
767 paleoclimatic changes in southern Sweden since the late glacial: the Hässeldala Port lake
768 sediment record, J. Paleolimnol., 50, 57-70, 2013.

769 Korte, M., Donadini, F., Constable, C.G.: Geomagnetic field for 0–3 ka: 2. A new series of
770 time-varying global models, Geochemistry Geophysics Geosystems (G3), 10, Q06008, doi:
771 10.1029/2008GC002297, 2009.

772 Lamb, H. H.: The early medieval warm epoch and its sequel, Palaeogeogr. Palaeoclimatol.
773 Palaeoecol., 1, 13–37, 1965.

774 Lambert, J, and Levret-Albaret, A.: Mille ans de séismes en France. Catalogues d'épicentres,
775 paramètres et references, Ouest-Editions, Presses Académiques, Nantes. 1996.

776 Lapointe, F., Francus, P., Lamoureaux, S.F., Saïd, M. and Cuven, S.: 1,750 years of large
777 rainfall events inferred from particle size at East Lake, Cape Bounty, Melville Island, Canada,
778 Journal of Paleolimnology, 48(1), 159–173, 2012.

779 Lionello, P., Abrantes, F., Congedi, L., Dulac, F., Gacic, M., Gomis, D., Goodess, C., Hoff,
780 H., Kutiel, H., Luterbacher, J., Planton, S., Reale, M., Schröder, K., Struglia, M.V., Toreti, A.,
781 Tsimplis, M., Ulbrich, U. and Xoplaki, E.: Introduction: Mediterranean Climate: Background
782 Information in Lionello P. (Ed.) The Climate of the Mediterranean Region. From the Past to
783 the Future, Amsterdam: Elsevier (Netherlands), XXXV-lXXX, 2012.

784 Lurcock, P. C. and Wilson, G. S.: PuffinPlot: A versatile, user-friendly program for
785 paleomagnetic analysis, Geochemistry, Geophysics, Geosystems, 13, Q06Z45, 2012.

786 Luterbacher, J., García-Herrera, R., Akcer-On, S., Allan, R., Alvarez-Castro, M. C., Benito,
787 G., Booth, J., Büntgen, U., Cagatay, N., Colombaroli, D., Davis, B., Esper, J., Felis, T.,
788 Fleitmann, D., Frank, D., Gallego, D., Garcia-Bustamante, E., Glaser, R., González-Rouco,
789 J.F., Goosse, H., Kiefer, T., Macklin, M.G., Manning, S., Montagna, P., Newman, L., Power,
790 M.J., Rath, V., Ribera, P., Riemann, D., Roberts, N., Sicre, M., Silenzi, S., Tinner, W.,
791 Valero-Garces, B., van der Schrier, G., Tzedakis, C., Vannière, B., Vogt, S., Wanner, H.,
792 Werner, J.P., Willett, G., Williams, M.H., Xoplaki, E., Zerefos, C.S. and Zorita, E.: A review
793 of 2000 years of paleoclimatic evidence in the Mediterranean, In: Lionello, P. (Ed.), The

794 Climate of the Mediterranean region: from the past to the future, Elsevier, Amsterdam, The
795 Netherlands, 87-185, 2012.

796 Miramont, C., Jorda, M. and Pichard, G.: Évolution historique de la morphogenèse et de la
797 dynamique fluviale d'une rivière méditerranéenne : l'exemple de la moyenne Durance
798 (France du sud-est), Géographie physique et Quaternaire,52(3), 381-392, 1998.

799 Moernaut, J., M. De Batist, F. Charlet, K. Heirman, E. Chapron, M. Pino, R. Brümmer and R.
800 Urrutia, Giant earthquakes in South-Central Chile revealed by Holocene mass-wasting events
801 in Lake Puyehue, Sediment. Geol., 195, 239–256, 2007.

802 Moernaut, J., Van Daele, M., Heirman, K., Fontijn, K., Strasser, M., Pino, M., Urrutia R., and
803 De Batist, M.: Lacustrine turbidites as a tool for quantitative earthquake reconstruction: New
804 evidence for a variable rupture mode in south central Chile, J. Geophys. Res. Solid Earth,
805 119, doi:10.1002/2013JB010738, 2014.

806 Monecke, K., Anselmetti, F.S., Becker, A., Sturm, M. and Giardini, D.: The record of historic
807 earthquakes in lake sediments of Central Switzerlanc, Tectonophysics, 394, 21–40, 2004.

808 Munich Re Group: Annual Review: Natural Catastrophes 2002, Munich Re Group, Munich,
809 Germany, 2003.

810 Moreno, A., Valero-Garces, B.L., Gonzalez-Samperiz, P. and Rico, M.: Flood response to
811 rainfall variability during the last 2000 years inferred from the Taravilla Lake record (Central
812 Iberian Range, Spain), J. Palaeolimnol., 40, 943–961, 2008.

813 Noren, A.J., Bierman, P.R., Steig, E.J., Lini, A. and Southon, J.: Millennial-scale storminess
814 variability in the northeastern United States during the Holocene epoch, Nature, 419, 821-824,
815 2002.

816 Oslegger, D.A., Heyvaert, A.C., Stoner, J.S. and Verosub, K.L.: Lacustrine turbidites as
817 indicators of Holocene storminess and climate: Lake Tahoe, California and Nevada, J
818 Paleolimnol., 42:103–122, 2009.

819 Page, M.J., Trustrum, N.A. and DeRose, R.C.: A high resolution record of storm-induced
820 erosion from lake sediments, New Zealand, Journal of Paleolimnology, 11, 333-348, 1994.

821 Parajka, J., Kohnová, S., Bálint, G., Barbuc, M., Borga, M., Claps, P., Cheval, S., Dumitrescu,
822 A., Gaume, E., Hlavčová, K., Merz, R., Pfaundler, M., Stancalie, G., Szolgay, J., Blöschl, G.:
823 Seasonal characteristics of flood regimes across the Alpine–Carpathian range, J. of
824 Hydrology, 394,78–89, 2010.

825 Passega, R.: Grain-size representation by CM patterns as a geological tool, J. of Sedimentary
826 Petrology, 34(4), 830–847, 1964.

827 Plaut, G., Schuepbach, E. and Doctor, M. Heavy precipitation events over a few Alpine sub-
828 regions and the links with large-scale circulation, 1971–1995, Climate Research, 17, 285–302,
829 2009.

830 Raible, C.C., Yoshimori, M., Stocker, T.F. and Casty, C.: Extreme midlatitude cyclones and
831 their implications for precipitation and wind speed extremes in simulations of the Maunder
832 Minimum versus present day conditions. Clim. Dyn. 28, 409–423, 2007.

833 Rajczak, J., Pall, P. and Schär, C.: Projections of extreme precipitation events in regional
834 climate simulations for Europe and the Alpine Region, J. Geophys. Res. Atm., 118, 1–17,
835 2013.

836 Reimer, P.J., Bard, E., Bayliss, A., Beck, J.W., Blackwell, P.G., Bronk Ramsey, C., Buck,
837 C.E., Cheng, H., Edwards, R.L., Friedrich, M., Grootes, P.M., Guilderson, T.P., Haflidason,
838 H., Hajdas, I., Hatt, C., Heaton, T.J., Hogg, A.G., Hughen, K.A., Kaiser, K.F., Kromer, B.,
839 Manning, S.W., Niu, M., Reimer, R.W., Richards, D.A., Scott, E.M., Southon, J.R., Turney,
840 C.S.M. and van der Plicht, J.: IntCal13 and MARINE13 radiocarbon age calibration curves 0-
841 50000 years calBP, Radiocarbon, 55(4), 1869–1887, 2013.

842 Russell, J.M., Vogel, H., Konecky, B.L., Bijaksana, S., Huang, Y., Melles, M., Wattrus, N.,
843 Costa, K. and King, J.W.: Glacial forcing of central Indonesian hydroclimate since 60,000 y
844 B.P., Proc .Nat. Acad. Sci. 111, 5100-5105, 2014.

845 Sauerbrey, M. A., Juschus, O., Gebhardt, A. C., Wennrich, V., Nowaczyk, N. R. and Melles,
846 M.: Mass movement deposits in the 3.6Ma sediment record of Lake Elgygytgyn, Far East
847 Russian Arctic, Climate of the Past 9, 1949–1967, 2013.

848 Schiefer, E., Gilbert, R. and Hassan, M.A.: A lake sediment-based proxy of floods in the
849 Rocky Mountain Front Ranges, Canada, Journal of Paleolimnology, 45, 137–149, 2011.

850 Schulte, L., Peña, J.C., Carvalho, F., Schmidt, T., Julià, R., Llorca, J. and Veit, H.: A 2600-
851 year history of floods in the Bernese Alps, Switzerland: frequencies, mechanisms and climate
852 forcing, Hydrol. Earth Syst. Sci., 19, 3047–3072, 2015.

853 Schwartz, S., Tricart, P., Lardeaux, J.M., Guillot, S. and Vidal, O.: Late tectonic and
854 metamorphic evolution of the Piedmont accretionary wedge(Queyras Schistes lustrés, western

Alps): Evidences for tilting during Alpine collision, Geol. Soc. Ame. Bull., 121, 502-518, 2009.

Scotti, O., Baumont, D., Quenet, G. and Levret, A.: The French macroseismic database SISFRANCE: objectives, results and perspectives, Annals of Geophysics, 47(2), 571-581, 2004.

Servonnat, J., Yiou, P., Khodri, M., Swingedouw, D., Denvil, S.: Influence of solar variability, CO2 and orbital forcing during the last millennium in the IPSLCM4 model, Clim. Past, 6, 445-460, 2010.

Simonneau, A., Chapron, E., Vannière, B., Wirth, S.B., Gilli, A., Giovanni, C. Di., Anselmetti, F. S., Desmet, M. and Magny M.: Mass-movement and flood-induced deposits in Lake Ledro, southern Alps, Italy: implications for Holocene palaeohydrology and natural hazards, Clim. Past 9, 825-840, 2013.

Sivan, O., Miramont, C., Pichard, G. and Prosper-Laget, V. : Les conditions climatiques de la torrentialité au cours du Petit Age Glaciaire de Provence, Archeologie du Midi Medieval, 26, 157–168, 2009.

Stockmarr, J.: Tablets with spores used in absolute pollen analysis. Pollen Spores 13, 615–621, 1971.

Støren, E.N., Olaf Dahl, S., Nesje, A. and Paasche Ø.: Identifying the sedimentary imprint of high-frequency Holocene river floods in lake sediments: development and application of a new method, Quat. Sci. Rev., 29, 3021-3033, 2010.

Strasser, M., Hilbe, M. and Anselmetti, F.S.:, Mapping basin-wide subaquatic slope failure susceptibility as a tool to assess regional seismic and tsunami hazards, Mar. Geophys. Res., 32, 331–347, 2011.

Sturm, M. and Matter, A.: Turbidites and varves in Lake Brienz (Switzerland): deposition of clastic detritus by density currents, Int. Assoc. Sedimentol. Spec. Publ., 2, 147–168, 1978.

Swierczynski, T., Lauterbach, S., Dulski, P., Delgado, J., Merz, B. and Brauer, A.: Mid- to late Holocene flood frequency changes in the northeastern Alps as recorded in varved sediments of Lake Mondsee (Upper Austria), Quat. Sci. Rev., 80, 78–90, 2013.

Thorndycraft, V.R. and Benito, G.: Late Holocene chronology of Spain: the role of climatic variability and human impact, Catena, 66, 34–41, 2006.

Torres, N.T., Och, L.M., Hauser, P.C., Furrer, G., Brandl, H., Vologina, E., Sturm, M., and Bürgmann, H. z Müller, B.: Early diagenetic processes generate iron and manganese oxide layers in the sediments of Lake Baikal, Siberia, Env. Sci.: Processes Impacts, 16, 879–889, 2014.

Trigo, I.F. and Davies, T.D.: Decline in Mediterranean rainfall caused by weakening of Mediterranean cyclones, Geophysical Research Letters, 27(18), 2913–2916, 2000.

Van Daele, M., Versteeg, W., Pino, M., Urrutia, R. and De Batist, M.: Widespread deformation of basin-plain sediments in Aysén fjord [Chile] due to impact by earthquake-triggered, onshore-generated mass movements, Marine Geol., 337, 67–79, 2013.

Van Daele, M., Moernaut, J., Doom, L. , Boes, E. , Fontijn, K., Heirman, K. , Vandoorne, W., Hebbeln, D., Pino, M., Urrutia, R., Brümmer, R. and De Batist, M.: A comparison of the sedimentary records of the 1960 and 2010 great Chilean earthquakes in 17 lakes: Implications for quantitative lacustrine palaeoseismology, Sedimentology, 62(5): 1466–1496, 2015.

Van Geel, B. and Aptroot, A.: Fossil ascomycetes in Quaternary deposits. Nova Hedwig 82, 313–329, 2006.

Van Geel, B., Buurman, J., Brinkkemper, O., Schelvis, J., Aptroot, A., van Reenen, G. and Hakjbilj, T.: Environmental reconstruction of a Roman period settlement site in Uitgeest (The Netherlands), with special reference to coprophilous fungi. J. Archaeol. Sci. 30, 873–883, 2003.

Wilhelm, B., Arnaud, F., Sabatier, P., Crouzet, C., Brisset, E., Chaumillon, E., Disnar, J.R., Guiter, F., Malet, E.,Reyss, J.L., Tachikawa, K., Bard, E. and Delannoy, J.J.: 1400 years of extreme precipitation patterns over the Mediterranean French Alps and possible forcing mechanisms, Quat. Res., 78, 1–12, 2012a.

Wilhelm, B., Arnaud, F., Enters, D., Allignol, F., Legaz, A., Magand, O., Revillon, S., Giguet-Covex, C. and Malet, E.: Does global warming favour the occurrence of extreme floods in European Alps? First evidences from a NW Alps proglacial lake sediment record, Clim. Change., 113, 563–581, 2012b.

Wilhelm, B., Arnaud, F., Sabatier, P., Magand, O., Chapron, E., Courp, T., Tachikawa, K., Fanget, B., Malet, E., Pignol, C., Bard, E. and Delannoy, J.J.: Palaeoflood activity and climate change over the last 1400 years recorded by lake sediments in the NW European Alps, J. Quat. Sci., 28, 189–199, 2013.

916 Wilhelm, B., Sabatier, P. and Arnaud, F.: Is a regional flood signal reproducible from lake
917 sediments? Sedimentology, 62(4), 1103–1117. 2015.

918 Wirth S.B., Glur, L., Gilli, A. and Anselmetti, F.S.: Holocene flood frequency across the
919 Central Alps – solar forcing and evidence for variations in North Atlantic atmospheric
920 circulation, Quatern. Sci. Rev., 80, 112–128, 2013a.

921 Wirth, S.B., Gilli, A., Simonneau, A., Ariztegui, D., Vannière, B., Glur, L., Chapron, E.,
922 Magny, M. and Anselmetti, F.S.: A 2000-year long seasonal record of floods in the southern
923 European Alps. Geophys. Res. Let., 40(15), 4025-4029, 2013b.
924

BE nr.	Core	Core depth (cm)	Core depth in core FOR13P2 (cm)	Event-free depth in core FOR13P2 (cm)	Material	^{14}C yrs. BP	Cal yrs. BP (±2σ)	Cal yrs. AD (±2σ)
2094.1.1	FOR13P4	84-85	82-83	33	Terrestrial plant remains	650 ± 18	561-665	1285-1389
2095.1.1	FOR13P4	109-111	106-108	46 ± 0.5		1052 ± 33	923-1052	898-1027
2096.1.1	FOR13P4	113-115	110-112	47 ± 0.5		1242 ± 66	1004-1292	658-946

Table 1. Radiocarbon dates of core FOR13P4. We calculated the event-free sedimentary depth by removing the graded beds, which were considered to be instantaneous deposits. See text for explanation, nature of samples and calibration procedures.

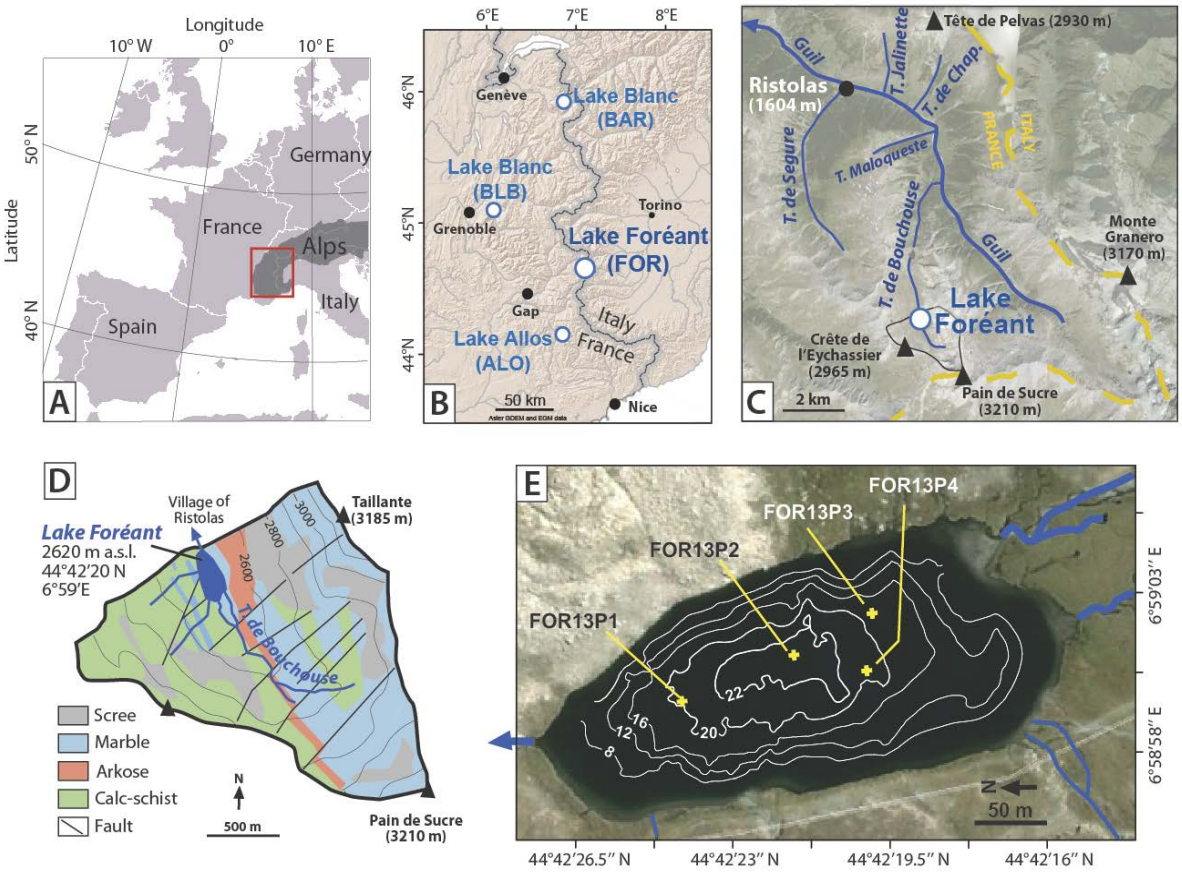

Figure 1. (A) Location of Lake Foréant in the Western Alps, (B) compared to the locations of the previously studied Lakes Blanc (BLB, Wilhelm et al., 2012b; BAR, Wilhelm et al., 2013) and Lake Allos (ALO, Wilhelm et al., 2012a). (C) Location of the Foréant catchment area in the hydrological network flowing to the village of Ristolas. (D) Geological and geomorphological characteristics of the Foréant catchment area. (E) Bathymetric map of Lake Foréant and coring sites.

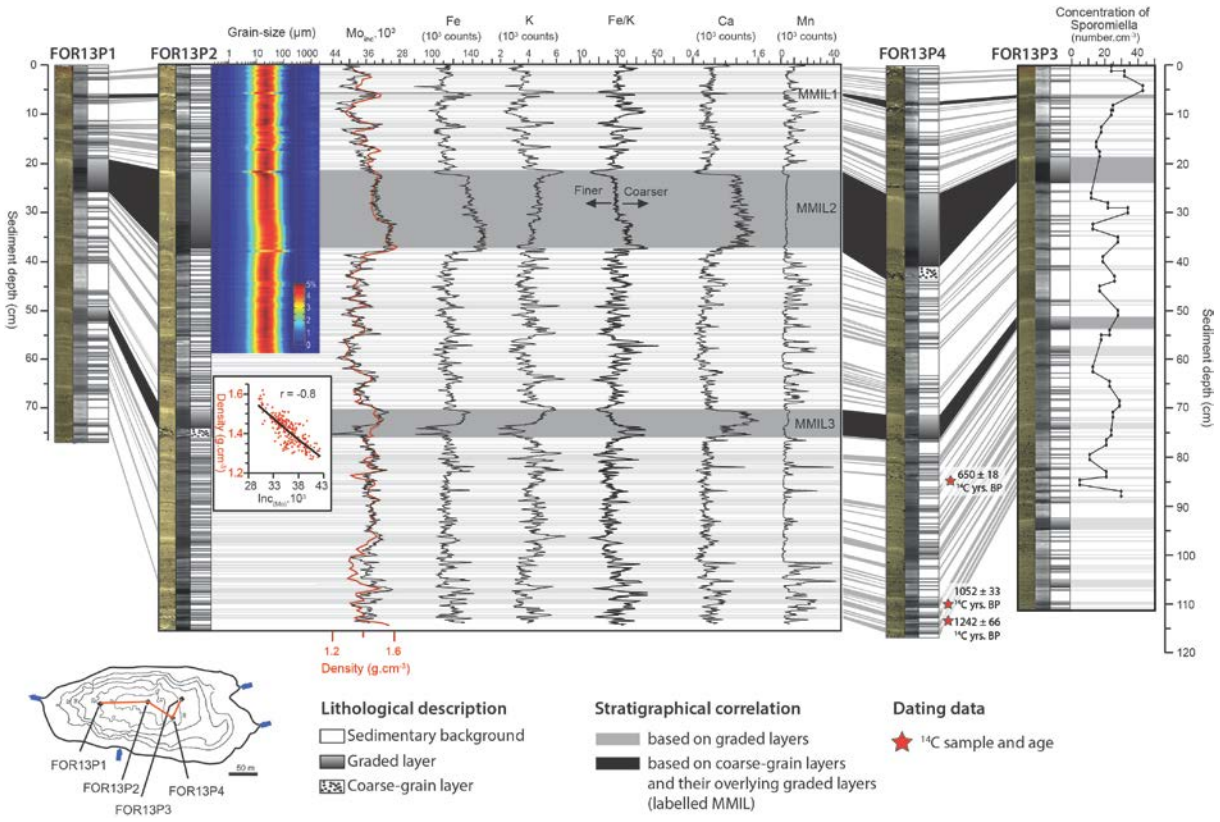

939

940 Figure 2. Lithological descriptions of cores and stratigraphic correlations based on
941 sedimentary facies. For each core, a photography (left), a X-ray image (center) and a
942 stratigraphic log is shown (right). ^{14}C samples are indicated by red stars. Variability in grain-
943 size distribution and geochemical elements (Fe, K, Ca and Mn) is shown for the core
944 FOR13P2. Mo_{inc} used as a high-resolution proxy of density is shown close to the density
945 measurements performed by gamma-ray attenuation. Variability in Sporomiella concentration
946 is shown for core FOR13P3.

947

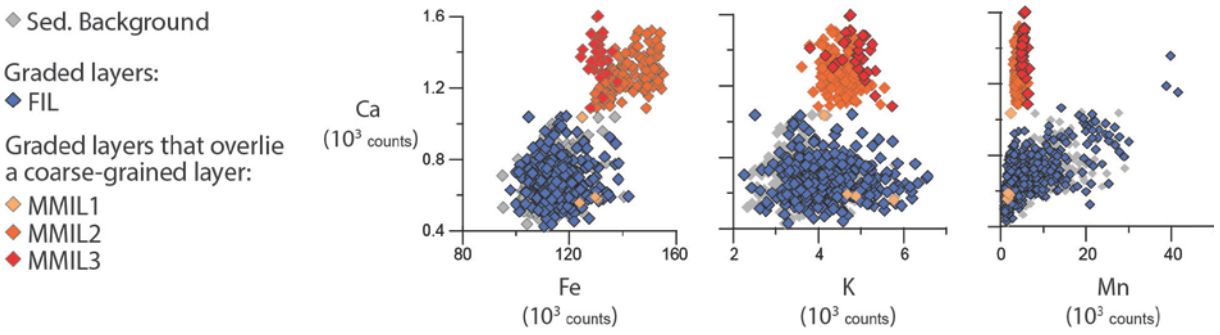

948

949 Figure 3. To illustrate the different geochemical characteristics of the sedimentary
950 background and the graded layers, their Ca intensities were plotted against their Fe, K and Mn

intensities. FIL refers to flood- and MMIL to mass-movement-induced layers. The different MMILs are labelled according to figure 2.

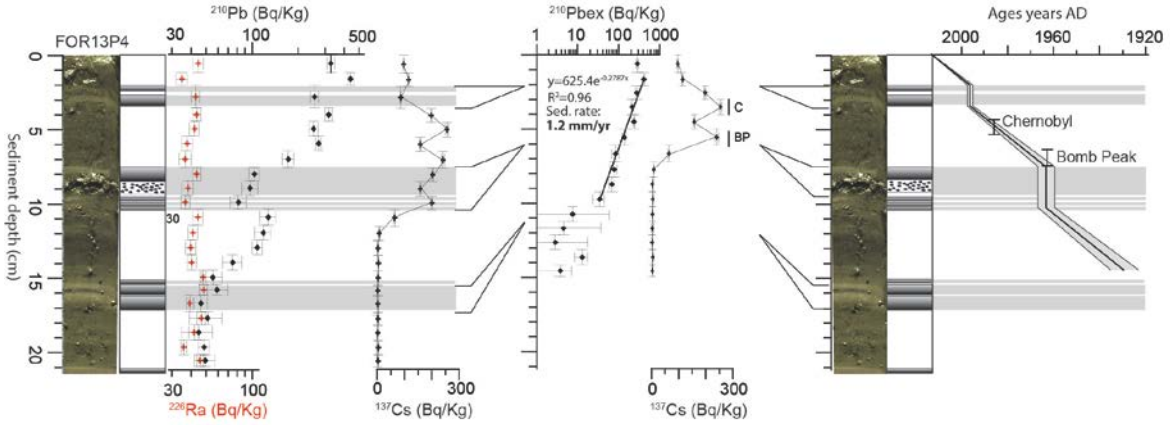

Figure 4. (A) ^{226}Ra, ^{210}Pb and ^{137}Cs profiles for core ALO09P12. (B) Application of a CFCS model to the event-free sedimentary profile of ^{210}Pb in excess (without the thick graded beds considered as instantaneous deposits). (C) Resulting age–depth relationship with 1σ uncertainties and locations of the historic ^{137}Cs peaks supporting the ^{210}Pb-based ages. C corresponds to the historic ^{137}Cs peak of Chernobyl (AD 1986) and MP to the maximum ^{137}Cs peak of the nuclear fallout (AD 1963).

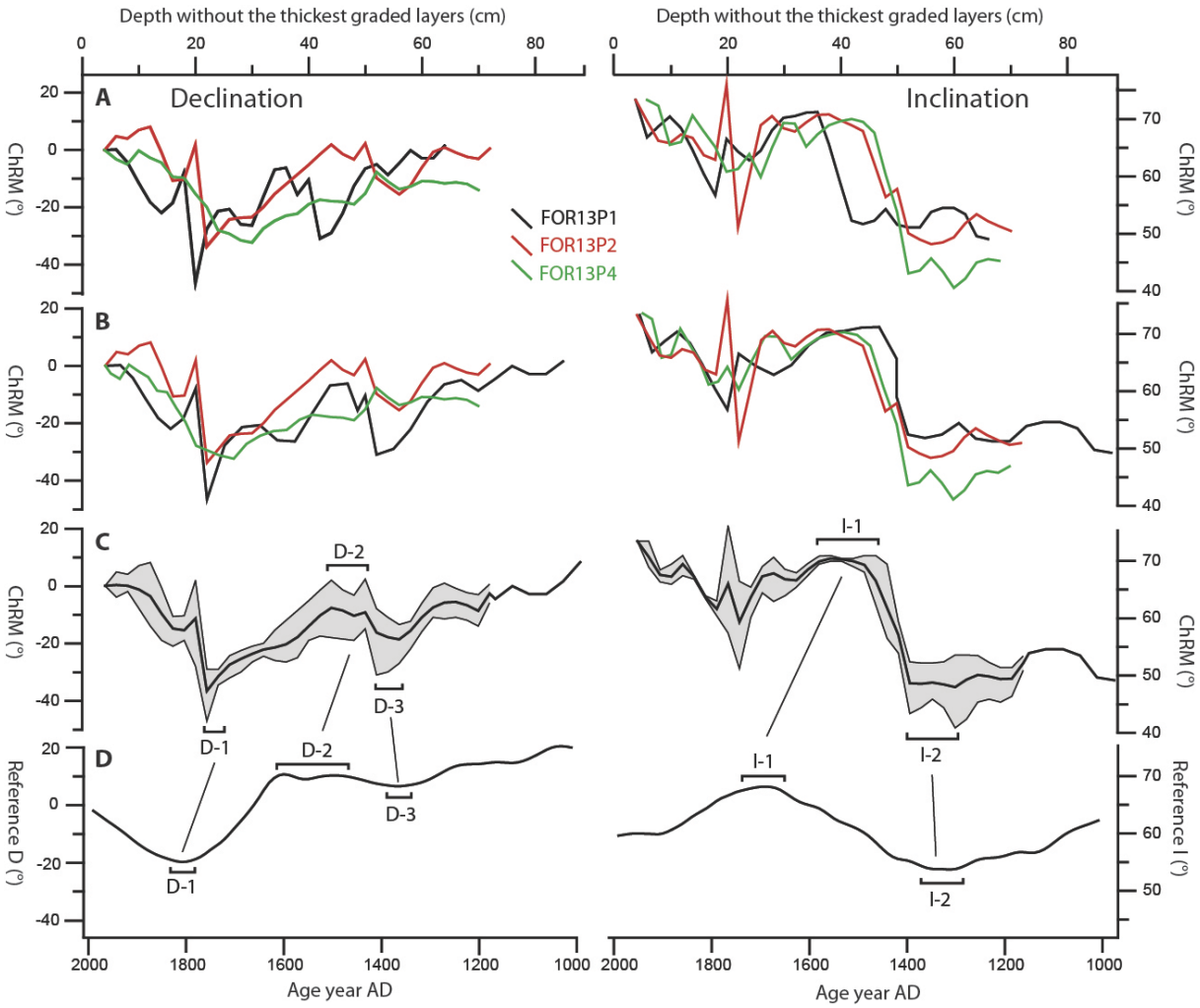

Figure 5. (A) Raw declination and inclination profiles of cores FOR13P1, FOR13P2 and FOR13P4. (B) The same profiles after removal of the thickest graded beds (interpreted as event layers) and adjustment of the different specific-core depths to a common reference depth. (C) Average of profiles shown in (B). (D) Correlation to the ARCH3.4k model reference curve of declination and inclination (Donadini et al., 2009; Korte et al., 2009). ChRM means characteristic remanent magnetization. The well-correlated declination and inclination features are labelled D-x and I-x, respectively.

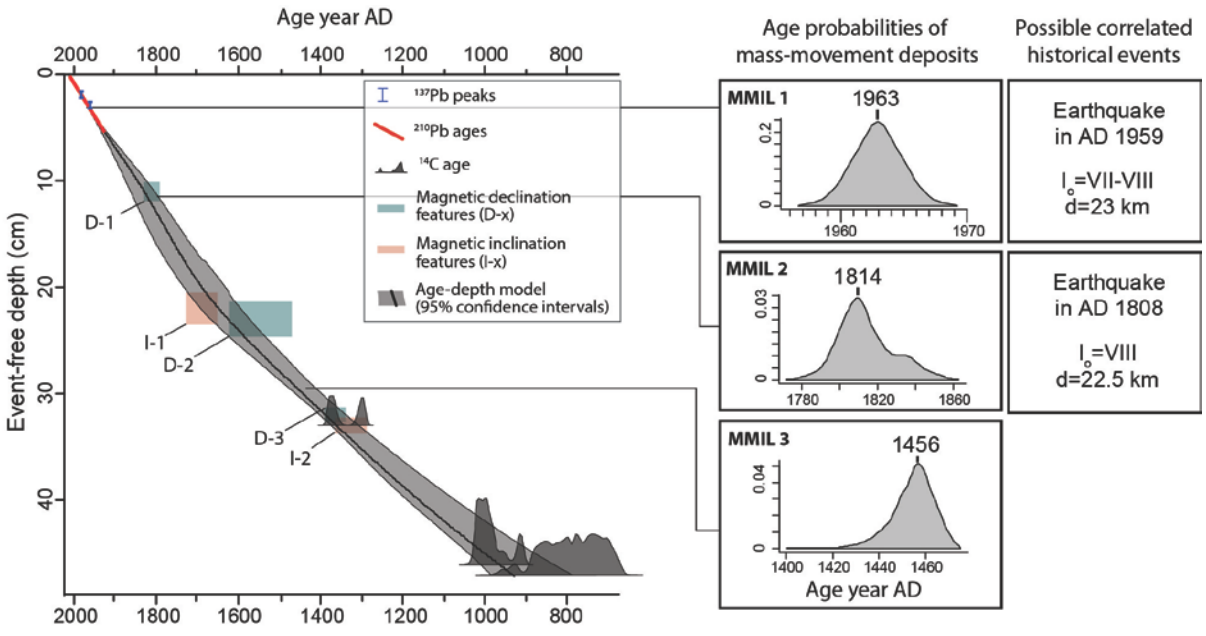

971

972 Figure 6. Age–depth model for core FOR13P2 calculated using the "clam" R-code package,
973 combining historic ^{137}Cs peaks, ^{210}Pb ages, calibrated ^{14}C ages and magnetic features on the
974 left side. Probability distribution frequencies of mass-movement ages and possible
975 correlations to historical earthquakes on the right side.

976

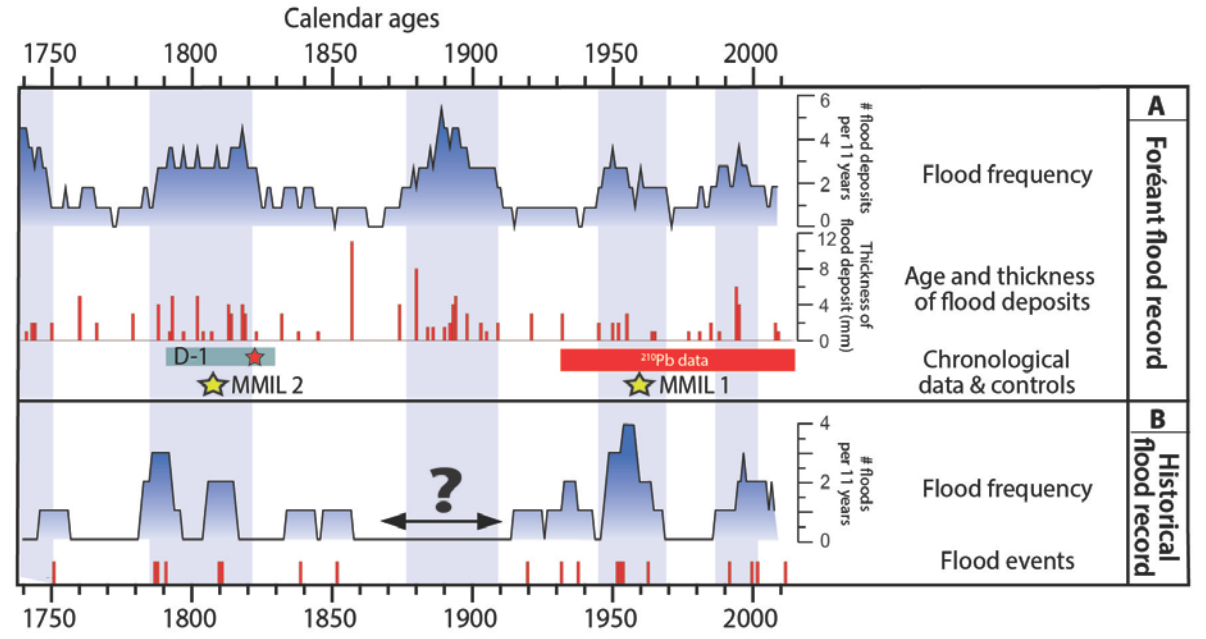

977

978 Figure 7. Comparison over the last 250 years of the reconstructed Foréant flood frequency
979 (11-yr running sum) and intensity (thickness of flood deposits) with the frequency (11-yr
980 running sum) of historical floods at Ristolas. The question mark refers to a possible gap in the
981 historical data.

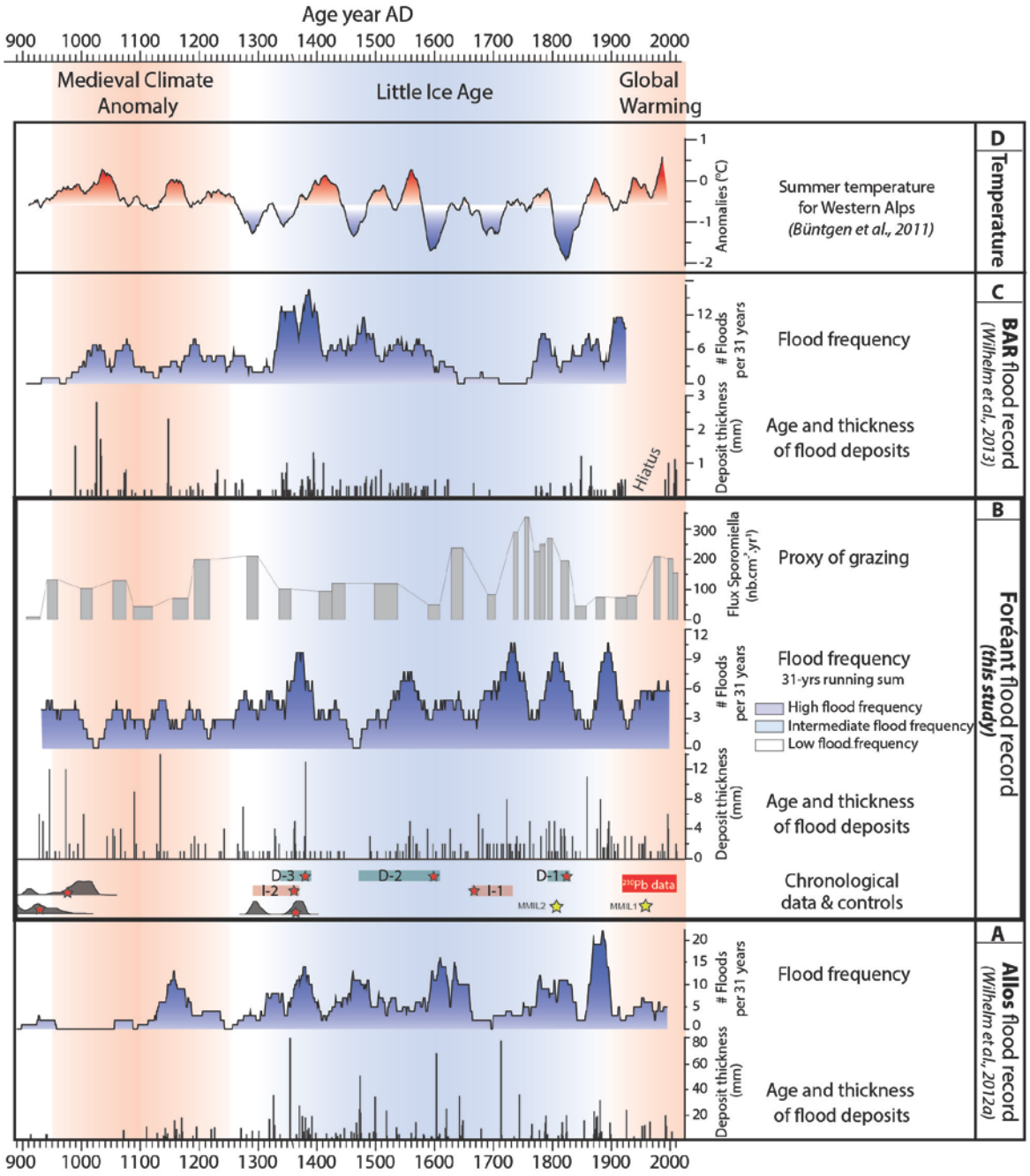

Figure 8. Comparison over the last millennium of (B) the reconstructed Foréant flood frequency (31-yr running average) and intensity (thickness of flood deposits) with (A) the Allos flood record from the southern French Alps (Wilhelm et al., 2012a), (C) the BAR flood record from the northern French Alps (Wilhelm et al., 2013) and (D) the tree-ring-based summer temperature for the European Alps (Büntgen et al., 2011). The reconstructed *Sporomiella*-type flux is also shown next to the Foréant flood record to highlight potential human impacts (i.e. grazing) on the erosion processes that might bias the flood record. The red stars below the Foréant record show the chronological markers with their 2-sigma uncertainty ranges.